Rotational relaxation of fluoromethane molecules in low-temperature collisions with buffer-gas helium

Xingjia Li, Liang Xu, Yanning Yin, Supeng Xu, Yong Xia,[*] and Jianping Yin[†]

State Key Laboratory of Precision Spectroscopy and Department of Physics, East China Normal University, Shanghai 200062, China

We propose a method to study the rotational relaxation of polar molecules [here taking fluoromethane (CH_3F) as an example] in collisions with 3.5 K buffer-gas helium (He) atoms by using an electrostatic guiding technique. The dependence of the guiding signal of CH_3F on the injected He flux and the dependence of the guiding efficiency of CH_3F on its rotational temperature are investigated both theoretically and experimentally. By comparing the experimental and simulated results, we find that the translational and rotational temperatures of the buffer-gas cooled CH_3F molecules can reach to about 5.48 and 0.60 K, respectively, and the ratio between the translational and average rotational collisional cross sections of CH_3F-He is $\gamma = \sigma_t/\sigma_r = 36.49 \pm 6.15$. In addition, the slowing, cooling, and boosting effects of the molecular beam with different injected He fluxes are also observed and their forming conditions are investigated in some detail. Our study shows that our proposed method can not only be used to measure the translational and rotational temperatures of the buffer-gas cooled molecules, but also to measure the ratio of the translational collisional cross section to the average rotational collisional cross section, and even to measure the average rotational collisional cross section when the translational collisional cross section is measured by fitting the lifetime of molecule signal to get a numerical solution from the diffusion equation of buffer-gas He atoms in the cell.

I. INTRODUCTION

The buffer-gas cooling technique is based on collisional cooling of thermal molecules (atoms) with cold buffer gas, which works by dissipating the energy of the molecular (atomic) ensemble via elastic collisions with cryogenically cooled helium (or neon) atoms, and directly cools molecules into the kelvin-temperature regime [1]. In 1998 the first cold molecule trapping was performed with $^2\Sigma$ calcium hydride (CaH) molecules, and about 10^8 molecules were loaded into a magnetic trap using buffer-gas loading [2]. The buffer-gas beams offer some significant applications in a variety of areas, such as direct laser cooling of diatomic molecules [3–7], precision measurements of the electron electric dipole moment [8,9] and cold molecular collisions [10–15], and so on. The buffer-gas cooling mechanism does not depend on the internal energy levels of molecules, so it is suitable for the cooling of nearly all kinds of neutral atoms or molecules. A key issue with the technique of buffer-gas cooling of molecules is the efficiency of cooling translational [16–20], rotational [21–23], vibrational [24], and spin [25,26] degrees of freedom. When thermal molecules are injected into a cryogenic cell, they will be continuously cooled and reach a thermal equilibrium during the collision with the buffer gas, and then the final translational and internal temperatures of the sample gases will be cooled to equal a temperature of the cryogenic helium gases, even lower [18]. Generally, collision-induced quenching is far more efficient for rotation degrees of freedom than the vibration one of molecules [27]. In a 4 K cell, both the translational and rotational thermalization occur with similar efficiency, typically the ratio between the translational

collisional cross section and average rotational collisional cross section is $\gamma = \sigma_t/\sigma_r = 10$–$100$ [18,21–23,27], and the rotational temperature in the extracted beam can reach ~ 1.0 K [18], which is significantly colder than the measured in-cell rotational temperature. However, the vibrational degrees of freedom have not been completely thermalized by cryogenically cooled helium atoms, indicating that compared with the translational or rotational degrees of freedom, thermalizing the vibrational degrees of freedom requires more collisions. Recently, Kozyryev and co-workers studied the vibrational relaxation of strontium monohydroxide (SrOH) molecules in collisions with 2 K He atoms [24], they found that the vibrational quenching proceeds relatively quickly, and efficiently thermalize vibrational degrees of freedom with low frequency vibrational modes ($\omega < 600\,\mathrm{cm}^{-1}$) at the time scales of <1 ms. The measured vibrational collisional quenching coefficient of $\gamma_{100} = \sigma_t/\sigma_v = 700$ was found in SrOH-He collisions. For the translational cooling of molecules, a typical helium-molecule diffusion elastic cross section is on the order of $\sim 10^{-14}$ cm^2 [1]. At low temperatures a typical rotational quench needs about 10–100 elastic collisions, while it needs more than 10^8 elastic collisions for a vibrational quench [27,28]. De Lucia and co-workers first measured the rotational cross sections of He-H$_2$S and He-NO over a 1–40 K temperature range [21,22]. Typical values were on the order of $5 \sim 10 \times 10^{-16}$ cm^2 at ~ 4 K, which is about 10–20 times smaller than a typical diffusive cross section at the same temperature.

Here we demonstrate a scheme to study a rotational relaxation of CH_3F molecules in low-temperature collisions with 3.5 K He atoms. The buffer gas effectively thermalizes the translational and rotational temperatures of the target molecules. The derived ratio between the translational collisional cross section and average rotational one of CH_3F-He is about 36. The slowing, cooling, and boosting effects of the

[*]yxia@phy.ecnu.edu.cn
[†]jpyin@phy.ecnu.edu.cn

guided molecular beam with different injected flux of helium are also observed. In Sec. II, the experimental setup and data acquisition are described. In Sec. III, the stark shift of CH_3F molecules in the external electric field is calculated. In Sec. IV, we characterize the electrostatically guided molecular beams that are cooled directly by the collisions of CH_3F with various fluxes of the cryogenically cooled He atoms and adiabatic cooling of the output CH_3F beam as the boosting effect appears. Some main results and conclusions are summarized in the final section.

II. EXPERIMENTAL APPARATUS AND DATA ACQUISITION

Our experiment is based on a copper buffer-gas cell that is thermally anchored to the cold head of a pulse-tube cooler (Cryomech PT415), which can keep the cell at a temperature of ∼ 3.5 K. Inside the cell, the CH_3F molecular beam is injected by a copper capillary pipe. In order to maintain a sufficiently high vapor pressure and avoid freezing of molecules, the molecular gas line is heated to a temperature of 215 K by a temperature controller.

The buffer-gas He atomic beam is continuously injected into the cell via the other gas fill line, which contains several windings to increase the length and reduces the heat conductance of the gas line to cool down the helium sufficiently. Since the He atoms need to be cooled down to 3.5 K before they enter into the cell, the buffer-gas fill line is tightly wound on the copper cylinder mounted on the first stage of the refrigerator for precooling of the helium gas to 33 K. It then enters into the volume enclosed by the outer radiation shield and mounted to the second stage of the refrigerator with a good thermal contact. The buffer-gas fill line consists of the copper pipe with a length of about 10 m and an outer and inner diameter of 2 mm and 1 mm, respectively; its good thermal contact and long, winding structure ensure that the helium beam is cooled down to 3.5 K before entering into the cell. The copper cell is a cuboid structure with an inner diameter of 25 mm and a length of 38 mm and surrounded by 3.5 K radiation shields, and the diameter of a nozzle at the cell outlet is 3 mm. Activated charcoal on the inner surface of the shields can absorb helium atoms and molecules to maintain high vacuum in the beam outlet area. When the refrigerator has reached 3.5 K, the pumping speed of activated charcoal is about 2.1×10^5 L/s, which is much more efficient than the turbo molecular pump. The injected gas flows are controlled by mass flow controllers and the flux adjust range is 0.05–5.00 standard cubic centimeters per minute at STP (SCCM). The He flow flux at the outlet of the cell is given by [1]

$$f_{out} = \frac{1}{4} n_{cell} \bar{v}_{cell} A_{aperture}, \qquad (1)$$

where n_{cell} and $\bar{v}_{cell}$ are the stagnation number density of the He atoms and the mean thermal velocity inside the cell, and $A_{aperture}$ is the exit area of the cell. At the steady state $f_{out} = f_{in}$, where f_{in} is the injected He flux; therefore, the number density of the He atoms can be derived as

$$n_{cell} = \frac{4 f_{in}}{A_{aperture} v_{cell}}. \qquad (2)$$

Then by controlling the mass flow controller, an adjustable buffer-gas density of 1×10^{14} to 1×10^{16} cm^{-3} inside the cell can be obtained precisely.

Between the main chamber and the detection one there is a differential pumping stage to preserve a low background pressure in the detection chamber during the measurement process. The main chamber and the detection one are pumped by two turbo molecular pumps with a pumping speed of 1000 L/s and 80 L/s, respectively. In buffer-gas cooling experiments, with the increase of inputted He flux, the transverse and longitudinal velocities of the output molecular beam will be increased and its rotational temperature will be reduced due to the increasing collision number, and then both the changes of the transverse velocity and the rotational temperature will determine the guiding efficiency of the electrostatic quadrupole guide when the guiding voltage is unchanged. So in order to greatly reduce the influence of the transverse velocity on the guiding efficiency, two collimators with an aperture diameter of 2 mm are placed in front of the cell, and the gap between the first collimator and the buffer-gas cell is 13 mm. To extract cold polar molecules from the cell, a straight electrostatic quadrupole guide segment is placed in front of the exit aperture of the second collimator, as shown in Fig. 1. The gap between the second collimator and the first guide is about 2 mm to prevent discharge. The guide segment is made of four stainless steel rods with a diameter of 2 mm and a surface-surface separation of 1 mm, and a two-dimensional quadrupole field configuration is formed when positive and negative voltages are applied on the neighboring electrodes (see Fig. 1). The total electrostatic guide consists of two quadrupole segments, separated by a 1 mm gap. The first segment is located in the vacuum vessel with a length of 210 mm and the second segment is located in the high-vacuum detection region with a length of 340 mm. After being thermalized with 3.5 K helium and extracted out of the cell along with continuously flowing helium, the cold polar molecular beam is guided by a hollow electrostatic quadrupole field and then detected by quadrupole mass spectrometry (QMS, QMG 700). This analyzer with a time resolution of 500 μs provides an ion counter, which is used to determine the flux and density of the guided molecular beam. To distinguish the QMS signal from the background, the first segment of the guide is connected with two high-voltage switches (HTS 301, MOSFET Push-Pull Switch, Behlke). Transistor-transistor logic pulses generated by a DIO64 card are applied to set the high-voltage switches on (200 ms) and off (300 ms) repeatedly. After switching on the guiding electric fields, it takes a while until the QMS signal starts rising, i.e., until the fastest molecules arrive. This delay time corresponds to the time of flight (TOF) of the fastest molecules from the cell aperture to the QMS detection volume, and then a TOF signal is generated. The second segment of the guide is permanently switched on to avoid pickup currents on the QMS. Between the second segment of the guide and the ion source of the QMS, there is a grounded grid mesh for further protection. By switching the high voltage on and off repeatedly, TOF signals of guided molecules are generated as shown in Fig. 2(a). Based on the delay time, which is corresponding to the rising slope of the TOF signal after switching on the high voltage, the longitudinal velocity of molecules can be derived by differentiation [29,30]. The velocity distribution of
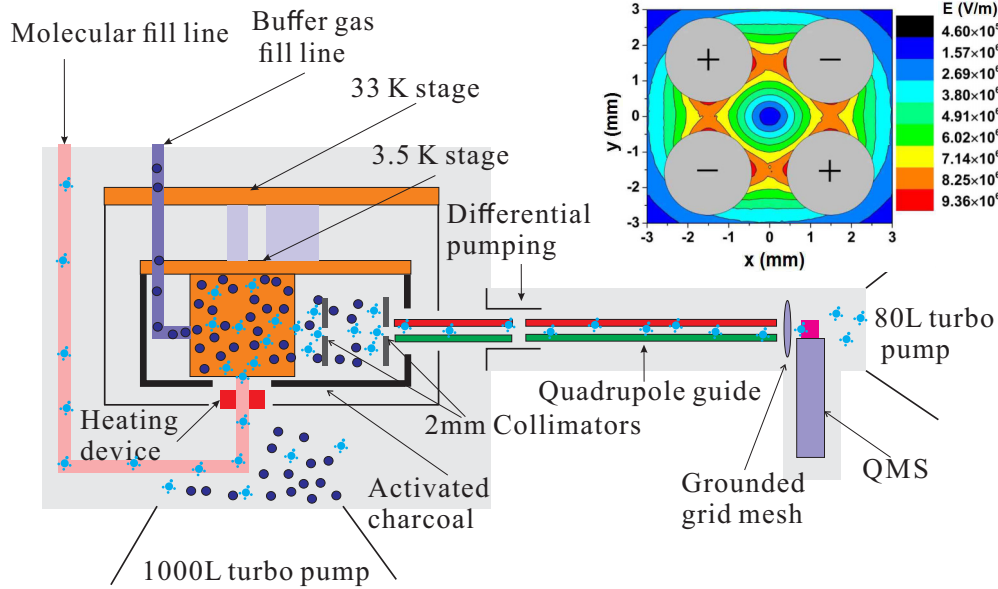
FIG. 1. Schematic diagram of buffer-gas cooling experimental setup. The helium is injected into the cell through the buffer-gas fill line which is thermally connected to the 33 and the 3.5 K stage, respectively. The heated molecular line is connected to a special inlet assembly, which has a bad thermal connection to the buffer-gas cell through a polyimide tube. This allows for the heating of the molecular fill line up to 215 K without affecting the temperature of the buffer-gas cell much. Outside of the buffer-gas cell, the helium atoms and molecules are pumped away by activated charcoal. After extracted from the buffer-gas cell, the molecular beam is first collimated by two collimators, then guided by two segments of quadrupole electric fields to the detection area and detected by QMS. The inset illustration in the upper right corner shows the electric field distribution of cross sectional area for ± 4 kV high voltage applied on the electrodes.
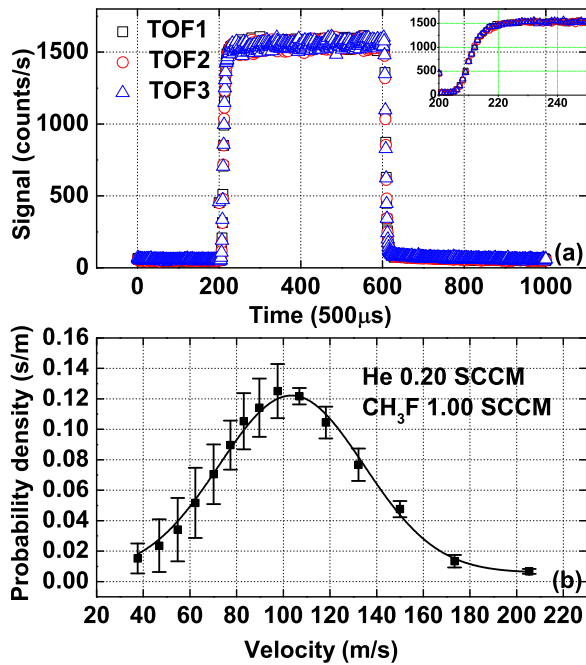
FIG. 2. (a) TOF signals of guided cold CH_3F beams; high voltages applied on the quadrupole guide are ± 4 kV, respectively. The inset illustration in the upper right corner shows the TOF rising slope after switching on the high voltage, which is applied on the first segment of the quadrupole guide. (b) Velocity distribution of guided cold CH_3F beams obtained by differentiation. The forward velocity of the maximum probability density is at 103 m/s and the FWHM of the velocity distribution is 73 m/s, corresponding to a translational temperature of 5.48 K. The error bars in the graph denote statistical errors.

the molecular beam can be derived from the TOF signal as follows [29]:

$$f(v) = \frac{S(t+\delta t) - S(t)}{\delta t} \frac{L}{v^2}, \qquad (3)$$

where S is the signal of the detected molecular beam, v is the velocity of the guided molecules, and L is the distance between the cell aperture and the detection area of QMS. Figure 2(b) shows the velocity distribution of the guided CH_3F molecules obtained from the TOF signal.

III. STARK SHIFT OF CH_3F IN AN EXTERNAL ELECTRIC FIELD

In order to manipulate cold molecules accurately, the response of the molecules to the external electric field, namely, the Stark effect, should be known. As we all know, the external electric field in the laboratory is much weaker than the molecular internal electric field, and its effect on the electron cloud distribution is negligible [31]. In the Born-Oppenheimer approximation, the period of nuclear vibration is shorter than that of nuclear rotation, so the dipole moment of the molecule in a given rotational state is the vibronic expectation value of the first moment of the charge. As follows, we will consider only the influence of the external fields on the molecular rotational levels. In this paper, a symmetrical top vibrational rotator is a very good approximation for CH_3F. The Hamiltonian of the CH_3F in absence of external fields is denoted by

$$H_0 = B_v J(J+1) + (A_v - B_v)K^2 - D_{vJ}J^2(J+1)^2$$
$$- D_{vJK}J(J+1)K^2 - D_{vK}K^4, \qquad (4)$$
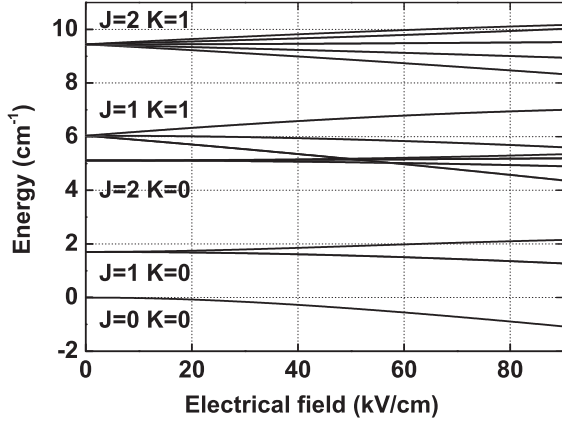
FIG. 3. The Stark shifts of the lowest rotational energies of CH_3F as a function of the applied electric field E. The five most abundant states (J, K, M) are indicated. The Stark shifts are obtained by numerically diagonalizing the Stark Hamiltonian $J = 0$–30.

and the eigenwave function of H_0 is $|JKM\rangle$, which is the symmetric top wave function, and can be expressed as

$$|JKM\rangle = \sqrt{\frac{2J+1}{8\pi^2}} \mathscr{D}_{MK}^{(J)*}(\phi,\theta,\chi), \qquad (5)$$

where A_v and B_v are the rotational constants along the a and b axes of the molecule in a given vibronic state; three centrifugal constants D_{vJ}, D_{vJK}, and D_{vK} have been introduced, which are much smaller than the rotational constants A_v and B_v. The K and M are the projections of J on the molecule-fixed z axis and the spaced-fixed internal field Z axis, respectively, and run from $-J$ to J. $\mathscr{D}_{MK}^{(J)*}(\phi,\theta,\chi)$ is the rotational operator matrices, and the Euler angles (ϕ,θ,χ) define the orientation of the space-fixed coordinates $(X, Y, \text{and } Z)$ with respect to the molecular coordinate frame $(x, y, \text{and } z)$ [32].

The calculation of the Stark effect needs the evaluation of the matrix elements as follows:

$$\langle J',K',M'|H_{\text{Stark}}|J,K,M\rangle$$
$$= \langle J',K',M'|-T^1(\mu)T_0^1(E)|J,K,M\rangle$$
$$= -E\sqrt{(2J+1)(2J'+1)}\sum_q (-1)^{M'-K'}T_1^q(\mu)$$
$$\times \begin{pmatrix} J' & 1 & J \\ -M' & q & M \end{pmatrix} \begin{pmatrix} J' & 1 & J \\ -M' & 0 & K \end{pmatrix}, \qquad (6)$$

where $T_1^q(\mu)$ are the components of the dipole moment vector μ in the molecular frame, which is the spherical tensor of rank 1. In Eq. (6), three J symbols give the selection rules naturally, and these rules indicate which states are coupled with each other. Then we can get the Stark shifts of the rotational levels in the presence of an external electric field, as Fig. 3 shows.

IV. MEASURED BEAM PROPERTIES

In buffer-gas cooling experiments, as we know, when the flux of the molecular sample is a constant, with an increase of the buffer-gas flux, the flux of the extracted molecular beam will be first increased and then become steady, and the

extraction should saturate [1] when

$$\gamma_{\text{cell}} \approx \frac{4}{9\pi}\frac{n_{\text{cell}}\sigma_t A_{\text{aperture}}}{L_{\text{cell}}} \approx 1, \qquad (7)$$

where n_{cell} is the buffer-gas density inside the cell, σ_t is the translational collisional cross section of CH_3F-He, and L_{cell} is the length of the buffer-gas cell. According to Eq. (7), when $A_{\text{aperture}} = \pi \times (1.5 \text{ mm})^2$, $L_{\text{cell}} = 38$ mm, and $\sigma_t = 2 \times 10^{14}/\text{cm}^2$, we find that $n_{\text{cell}} = 1.4 \times 10^{16}/\text{cm}^2$ of helium density inside the cell is needed to get the extraction saturation which corresponds to the helium flux of 7 SCCM for our experimental setup.

Figure 4(a) shows the dependence of the guiding signal of CH_3F on the injected flux of helium. We can find from Fig. 4(a) that when the injected He atomic flux is below 0.25 SCCM, the buffer-gas density is not high enough to extract the molecule species from the cell, the guided CH_3F signal will be increased with an increase of the injected helium flux f_{He}, and the number of thermalized and guided molecules extracted from the cell is about proportional to the square of f_{He}. While further increasing f_{He} and experiencing full thermalization, the guided molecules drop slowly, and the maximum signal can be obtained with a helium flux of 0.25 SCCM, corresponding
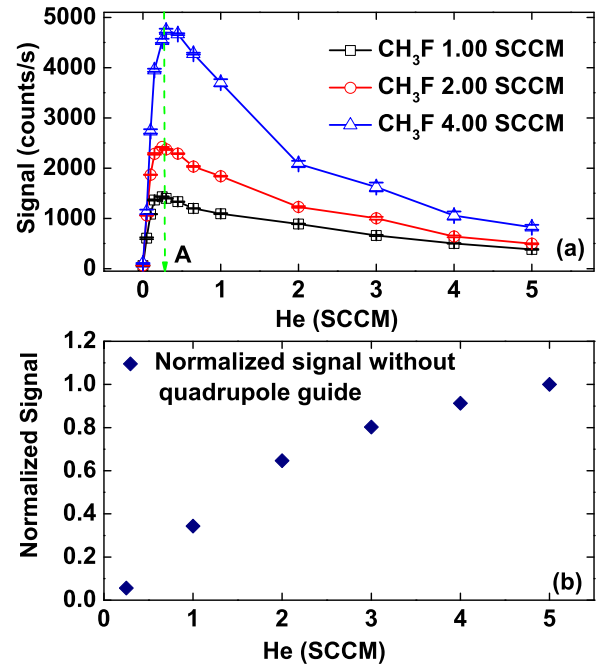
FIG. 4. (a) The dependence of the guided signal of CH_3F on the injected flux of helium. As the injected molecule flux is set to be 1.00, 2.00, and 4.00 SCCM, respectively, with an increase of the injected flux of helium from 0.05 to 5.00 SCCM, the signal of CH_3F detected by the QMS increases quickly and then drops slowly; the maximum QMS signal can be obtained with helium flux of 0.25 SCCM, which corresponds to the helium density of 5×10^{14} cm^{-3} inside the cell. The error bars in the graph denote statistical errors. (b) The dependence of the signal of CH_3F on the injected flux of helium without the quadrupole guide. The inputted flux of CH_3F is 2.00 SCCM, even when the injected helium flux is increased to 5.00 SCCM; the free flight signal of CH_3F detected by the QMS is still increasing with the increase of the inputted helium flux.

to a density of $n_{He} = 5 \times 10^{14}$ cm^{-3} inside the cell. However, after moving the guide away (i.e., without guiding) the free flight signal of CH$_3$F is detected by the QMS, and the results are shown in Fig. 4(b). We can find from Fig. 4(b) that the free flight signal of CH$_3$F is quite different; even when the injected helium flux is increased to 5.00 SCCM, the free flight signal of CH$_3$F still increases with the increasing of the inputted helium flux, which is consistent with other buffer-gas cooling results [1,17–19]. Barry *et al.* [18] and Hutzler *et al.* [19] found that the transverse velocity spread was increased with increasing buffer-gas flow; in particular, a typical divergent angle of output molecular beam is about 15°, which is about 1/4 rad from the centerline, that is, a typical transverse velocity is about 1/4 of the forward velocity. According to our measured results, with an increase of the inputted helium flux from 0.20 to 5.00 SCCM, the forward velocity of the guided CH$_3$F molecular beam is increased from 103 to 170 m/s, and the typical transverse velocity is increased from about 25.8 to 42.5 m/s. However, the total depth of the quadrupole guide is ~ 1 K for low J, which corresponds to ~ 20 m/s for CH$_3$F and smaller than the increased transverse velocity (25.8 to 42.5 m/s) of the output CH$_3$F molecular beam, so the influence of the increased transverse velocity on the guided signal of CH$_3$F cannot be ignored.

In order to greatly reduce this influence, two collimators with an aperture diameter of 2 mm are placed in front of the cell to reduce the influence of the increased transverse velocity of the molecular beam, as shown in Fig. 1. Two collimators are necessary since there are collisions near the beam aperture, which can make the effective source of molecules appear different from the aperture [33]. The first collimator is placed at 13 mm from the cell where collisions have been stopped. Our experimental result shows that the highest forward velocity of CH$_3$F is 170 m/s (obtained with an inputted helium flux of 5.00 SCCM), so the transverse velocity of the output molecular beam from the buffer-gas cell is about 42.5 m/s [18,19]. According to the results of Monte Carlo simulation, after being collimated by the two collimators, the transverse velocity of CH$_3$F is reduced to below 13 m/s (obtained with a forward velocity of 170 m/s) for all buffer-gas flow conditions, so the electrostatic guide can accept almost all weak-field-seeking (WFS) states CH$_3$F and the influence of the transverse velocity on guiding efficiency can be ignored after we place the two collimators in front of the buffer-gas cell.

After adding two collimators, we can conclude that the reduction of the guided molecule number in the detection area is caused by rotational cooling of the CH$_3$F molecule when the guiding voltage is unchanged and the injected helium flux is more than 0.25 SCCM, so the decreasing of the signal (i.e., the decreasing of the guiding efficiency of the WFS molecules in the electrostatic quadrupole field) after point A in Fig. 4(a) can be mainly caused by the reduction of the rotational temperature, which determines the rotational state population of CH$_3$F. That is to say, more molecules in the WFS states are transferred into ones in the strong-field-seeking state during the rotational relaxation process. In support of this claim, Monte Carlo simulations are carried out as follows [34]: for different rotational temperatures the state population ($J = 0$–30) of CH$_3$F can be obtained as seen in Fig. 5. In addition, with an external electric field of $E = 80$ kV/cm, there are totally
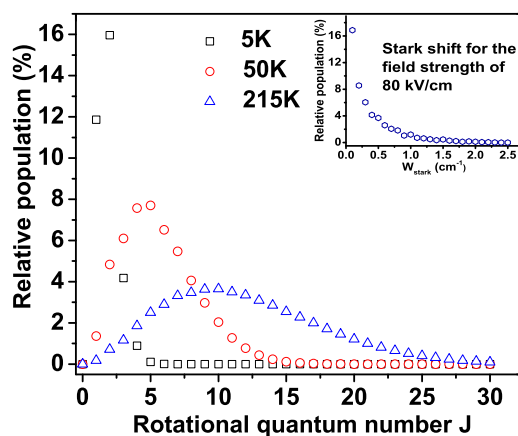
FIG. 5. Relative population (royal blue hexagon in the upper right corner) of WFS states of CH$_3$F vs Stark shift for the field strength of 80 kV/cm; the black squares, red circles, and blue triangles show the relative population of WFS states of CH$_3$F via the rotational energy level for $J = 0$–30 at rotational temperatures of 5, 50, and 215 K, respectively.

as many as 10 007 WFS states, as shown in Fig. 6, so it is necessary to simplify our simulations without changing the characters of guiding. In the guide, the changes of molecular velocities and positions mostly depend on Stark shift W_{Stark}. As the molecules with a larger W_{Stark} will suffer a larger gradient force and are apt to stay in the guide, we classify all the WFS states of the molecules into several tens of representative states according to their W_{Stark} (e.g., the states whose W_{Stark} is between 1.0 and 1.1 cm^{-1} are represented by the state with W_{Stark} as 1.05 cm^{-1}, such as the state $|16,11,-11\rangle$). So we can choose 25 representative states to represent all the WFS states with a W_{Stark} up to 2.5 cm^{-1}. The variation range of Stark shift represented by each representative state is ± 0.05 cm^{-1}, and the difference of Stark shifts between two adjacent representative states is defined as 0.1 cm^{-1}; then our Monte Carlo simulations for the electrostatically guided CH$_3$F molecules with the 10 007 WFS states are simplified to the simulations of CH$_3$F with 25 representative states. The guiding
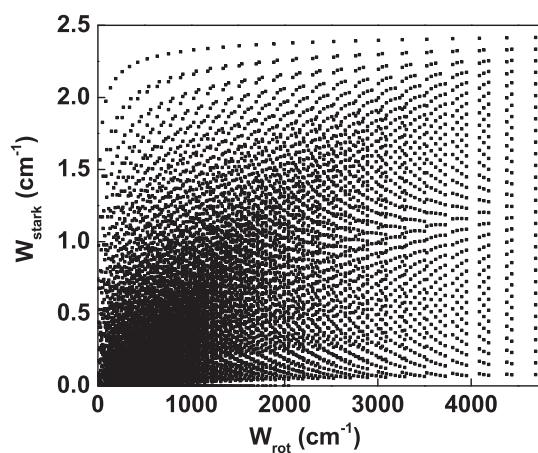
FIG. 6. The dependence of the Stark shift of the WFS state CH$_3$F molecule in 80 kV/cm external electric field on the rotational energy for the rotational quantum number of $J = 0$–30.
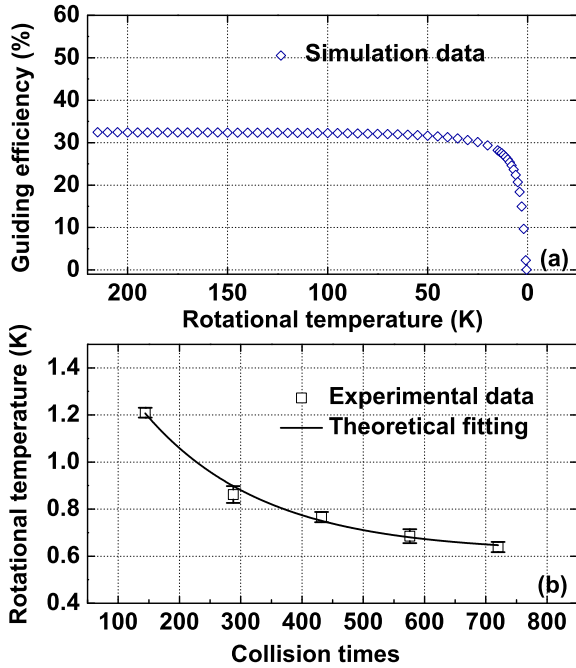
FIG. 7. (a) Monte Carlo simulated results show that for the CH_3F molecule beam, above 15 K the guiding efficiency of molecules in the quadrupole field is nearly not varied, but below 15 K the guiding efficiency decays quickly. (b) The relation between the rotational temperature and collision times. The data is obtained by comparing the experimental values with theoretical simulation results. Error bars in the graph denote statistical errors, and the curve is obtained by fitting $T_{rot}(N) = T_{lrot} + (T_{irot} - T_{lrot}) \times e^{-N/\gamma\kappa}$.

efficiency for each representative rotational state is obtained by straight quadrupole guide simulations. Then the total guiding efficiency for different rotational temperatures can be obtained. As shown in Fig. 7, when the rotational temperature of CH_3F is above 15 K, the guiding efficiency of cold molecules in the electrostatic quadrupole field is nearly not varying and the percentage of the WFS molecules is 47.21%. However, when the rotational temperature is below 15 K, there is a quick decrease of guiding efficiency as the rotational temperature drops from 15 to 1 K, and the percentage of the WFS molecules drops to 2.52% as the rotational temperature decreases to 1 K, which is consistent with our experimental results.

Inside the buffer-gas cooling cell, the density of helium is much larger than the density of molecules since most of the molecules are diffused to the cold cell wall and get lost. Therefore, the process of cold collisions is mainly determined by buffer-gas density. The mean free path of the molecule inside the cell is given by $\lambda = 1/\sqrt{2}n\sigma_t$, where n is the density of helium and σ_t is the translational elastic collision cross section of CH_3F-He. Based on the cell dimensions, when the injected flux of helium is 0.25 SCCM, the mean free path of the molecule inside the cell is ~ 0.7 mm; few collisions occurred near the cell aperture and the boosting effect is not obvious. The reduction of the temperature of the colliding molecules can be explained by the elastic scattering model of rigid spheres. According to energy and momentum conservation laws, after statistically averaging for a complete velocity distribution of the thermal molecules, it is easy to obtain a temperature change

of the molecular sample after each collision with the buffer gas; colliding N times with cold helium, the translational temperature [1] of CH_3F can be approximately expressed as

$$T_N = T_b + (T_i - T_b) \times e^{-N/\kappa}, \tag{8}$$

where T_b is the translational temperature of the helium and T_i is the initial translational temperature of the CH_3F molecule, and $\kappa \equiv (m_{molecule} + m_{helium})^2/2m_{molecule}m_{helium}$.

However, after being injected from the molecular fill line, CH_3F molecules undergo at least 36 times of collisions before being ejected from the cell aperture. After 36 times of collisions with 3.5 K cold helium, the translational temperature of the CH_3F molecules is $T_{36} \approx 3.74$ K, which means that 0.25 SCCM helium is sufficient to thermalize the translational temperature of CH_3F close to 3.5 K through cold collisions. When the injected flux of helium is increased from 1.00 to 5.00 SCCM, the guiding efficiency under the condition of high buffer-gas fluxes ($f_{He} > 0.25$ SCCM) can be calculated by comparing Figs. 4(a) and 4(b). Then the rotational temperature for different buffer-gas flux conditions can be obtained by its one-to-one correspondence with the guiding efficiency as shown in Fig. 7(a). Figure 7(b) shows the dependence of the rotational temperature of the guided molecules on collision times mainly determined by the buffer-gas density.

As we all know, it needs more collisions to thermalize the rotational temperature of molecules than their translational temperature. Besides, the lowest rotational temperature of the molecules could be much lower [18] than the temperature of the buffer-gas He atoms. Unlike elastic collisions, which govern translational relaxation, it is not easy to find a simple expression for the number of collisions necessary for rotational thermalization, because the rotational relaxation rates depend strongly on molecular structure, and for different relaxation channels and rotational state populations, the molecular rotational cross sections are different. However, for symmetric top molecules at specific rotational temperature, the rotational state population can be definite, therefore, different rotational cross sections can be replaced by an average one. In cryogenics cells, both translational and rotational thermalizations occur with similar efficiency [27]. Based on the model above, the rotational relaxation expression of CH_3F can be carried out on the analogy with the translational relaxation process, and the dependence of the rotational temperature of CH_3F on the collision times can be obtained by fitting the experimental data in Fig. 7(b) and given by

$$T_{rot}(N) = T_{lrot} + (T_{irot} - T_{lrot}) \times e^{-N/\gamma\kappa}, \tag{9}$$

where N is collision times, T_{irot} is the initial rotational temperature of CH_3F, T_{lrot} is the lowest rotational temperature of CH_3F that can be obtained by cold collisions and adiabatic cooling, $\kappa \equiv (m_{molecule} + m_{helium})^2/2m_{molecule}m_{helium}$, and γ is the ratio between the translational collisional cross section and the average rotational collisional cross section. By fitting the data in Fig. 7(b) with Eq. (9) above, the average ratio between the translational collisional cross section and the rotational collisional cross section $\gamma = \sigma_t/\sigma_r = 36.49 \pm 6.15$ can be obtained.

The molecular beam extracted from the cell exit can be operated both in an effusive regime and a hydrodynamically enhanced regime, mainly depending on the buffer-gas density.
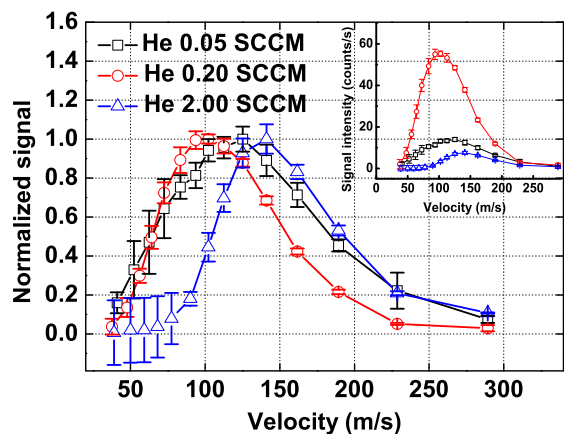
FIG. 8. Normalized velocity distribution of the CH_3F molecular beam with the injected CH_3F flux of 2.00 SCCM. When the injected helium flux is 0.05 SCCM, the velocity distribution is a typical effusive beam. As the injected helium flux is increased to 0.20 SCCM, cooling and slowing effects are obvious. With further increasing the injected helium flux to 2.00 SCCM, the CH_3F molecular beam is moving to the high speed region caused by the boosting effect.

The slowing, cooling, and boosting effects of the guided molecular beam with different injected fluxes of helium can be observed in Fig. 8. In order to clearly show these effects, we normalize the velocity distribution of the guided CH_3F molecular beam with the injected CH_3F flux of 2.00 SCCM. The inset illustration shows the dependence of the absolute guided signal intensity on the molecular velocity for different helium fluxes. When the injected He flux is 0.05 SCCM (corresponding to a helium density of 1×10^{14} cm^{-3}), CH_3F molecules undergo few collisions before being ejected out from the cell aperture, and then the cooling and slowing effects are not clear. When the injected He is increased to 0.20 SCCM, slowing and cooling effects are obvious compared with the injected He flux of 0.05 SCCM. With further increasing the He flux to 2.00 SCCM, the velocity distribution of the buffer-gas cooled CH_3F molecular beam moves to a high speed region caused by the boosting effect. The formed mechanism of the boosting effect in the high He flux region can be explained as follows: the rotational energy of CH_3F is transformed to the translational kinetic energy of CH_3F after tens of collisions

with He atoms near the cell nozzle, and then the rotational temperature of CH_3F is further decreased to about 0.60 K by adiabatic cooling after ejecting from the buffer-gas cell, so the lowest rotational temperature of the molecules can be lower, even much lower, than the temperature of the buffer-gas He atoms. This shows that our experimentally measured rotational temperature (0.60 K) of the output CH_3F beam is justifiable and believable.

V. CONCLUSIONS

In this paper, we have proposed an electrostatic guiding scheme to demonstrate the rotational relaxation of polar molecules (such as CH_3F) in low-temperature collisions with 3.5 K He atoms, and the dependence of the guiding efficiency of CH_3F on its rotational temperature is studied. We found that the translational and rotational temperatures of the buffer-gas cooled CH_3F molecules can be reached to about 5.48 and 0.60 K, respectively, and the ratio between the translational and average rotational collisional cross sections of CH_3F is about 36. Also, the slowing, cooling, and boosting effects of the guided molecular beam induced by the buffer-gas density has also been observed and studied. Our study shows that our proposed method can not only be used to measure the translational and rotational temperatures of the buffer-gas cooled molecules, but also to measure the ratio between the translational and average rotational collisional cross sections, and even to measure the average rotational collisional cross section when the translational collisional cross section is measured by fitting the lifetime of the molecule signal to get a numerical solution from the diffusion equation of the buffer-gas He atoms in the cell [35,36], and it should work for a large variety of polar molecules.

[1] N. R. Hutzler, H. I. Lu, and J. M. Doyle, The buffer gas beam: An intense, cold, and slow source for atoms and molecules, Chem. Rev. **112**, 4803 (2012).

[2] J. D. Weinstein, R. deCarvalho, T. Guillet, B. Friedrich, and J. M. Doyle, Magnetic trapping of calcium monohydride molecules at millikelvin temperatures, Nature (London) **395**, 148 (1998).

[3] E. S. Shuman, J. F. Barry, D. R. Glenn, and D. DeMille, Radiative Force from Optical Cycling on a Diatomic Molecule, Phys. Rev. Lett. **103**, 223001 (2009).

[4] E. S. Shuman, J. F. Barry, and D. DeMille, Laser cooling of a diatomic molecule, Nature (London) **467**, 820 (2010).

[5] M. T. Hummon, M. Yeo, B. K. Stuhl, A. L. Collopy, Y. Xia, and J. Ye, 2D Magneto-Optical Trapping of Diatomic Molecules, Phys. Rev. Lett. **110**, 143001 (2013).

[6] V. Zhelyazkova, A. Cournol, T. E. Wall, A. Matsushima, J. J. Hudson, E. A. Hinds, M. R. Tarbutt, and B. E. Sauer, Laser cooling and slowing of CaF molecules, Phys. Rev. A **89**, 053416 (2014).

[7] J. F. Barry, D. J. McCarron, E. B. Norrgard, M. H. Steinecker, and D. DeMille, Magneto-optical trapping of a diatomic molecule, Nature (London) **512**, 286 (2014).

[8] M. R. Tarbutt, B. E. Sauer, J. J. Hudson, and E. A. Hinds, Design for a fountain of YbF molecules to measure the electrons electric dipole moment, New J. Phys. **15**, 053034 (2013).

[9] J. Baron, W. C. Campbell, D. DeMille, J. M. Doyle, G. Gabrielse, Y. V. Gurevich, P. W. Hess, N. R. Hutzler, E. Kirilov, I. Kozyryev, B. R. O'Leary, C. D. Panda, E. S. Petrik, B. Spaun, A. C. Vutha,

and A. D. West, Order of magnitude smaller limit on the electric dipole moment of the electron, Science **343**, 269 (2014).

[10] B. C. Sawyer, B. K. Stuhl, M. Yeo, T. V. Tscherbul, M. T. Hummon, Y. Xia, J. Klos, D. Patterson, J. M. Doyle, and J. Ye, Cold heteromolecular dipolar collisions, Phys. Chem. Chem. Phys. **13**, 19059 (2011).

[11] J. K. Messer and F. C. De Lucia, Measurement of Pressure-Broadening Parameters for the CO-He System at 4 K, Phys. Rev. Lett. **53**, 2555 (1984).

[12] D. R. Willey, V. Choong, and F. C. De Lucia, Very low temperature helium pressure broadening of DCl in a collisionally cooled cell, J. Chem. Phys. **96**, 898 (1992).

[13] M. M. Beaky, T. M. Goyette, and F. C. De Lucia, Pressure broadening and line shift measurements of carbon monoxide in collision with helium from 1 to 600 K, J. Chem. Phys. **105**, 3994 (1996).

[14] T. J. Ronningen and F. C. De Lucia, Helium induced pressure broadening and shifting of HCN hyperfine transitions between 1.3 and 20 K, J. Chem. Phys. **122**, 184319 (2005).

[15] M. T. Hummon, T. V. Tscherbul, J. Kłos, Hsin-I Lu, E. Tsikata, W. C. Campbell, A. Dalgarno, and J. M. Doyle, Cold N+NH Collisions in a Magnetic Trap, Phys. Rev. Lett. **106**, 053201 (2011).

[16] S. E. Maxwell, N. Brahms, R. deCarvalho, J. S. Helton, S. Nguyen, D. Patterson, J. M. Doyle, D. R. Glenn, J. Petricka, and D. DeMille, High-Flux Beam Source for Cold, Slow Atoms or Molecules, Phys. Rev. Lett. **95**, 173201 (2005).

[17] D. Patterson and J. M. Doyle, Bright, guided molecular beam with hydrodynamic enhancement, J. Chem. Phys. **126**, 154307 (2007).

[18] J. F. Barry, E. S. Shuman, and D. DeMille, A bright, slow cryogenic molecular beam source for free radicals, Phys. Chem. Chem. Phys. **13**, 18936 (2011).

[19] N. R. Hutzler, M. F. Parsons, Y. V. Gurevich, P. W. Hess, E. Petrik, B. Spaun, A. C. Vutha, D. DeMille, G. Gabrielse, and J. M. Doyle, A cryogenic beam of refractory, chemically reactive molecules with expansion cooling, Phys. Chem. Chem. Phys. **13**, 18976 (2011).

[20] N. E. Bulleid, S. M. Skoff, R. J. Hendricks, B. E. Sauer, E. A. Hinds, and M. R. Tarbutt, Characterization of a cryogenic beam source for atoms and molecules, Phys. Chem. Chem. Phys. **15**, 12299 (2013).

[21] P. L. James, I. R. Sims, and I. W. M. Smith, Total and state-to-state rate coefficients for rotational energy transfer in collisions between NO ($X^2\Sigma$) and He at temperatures down to 15 K, Chem. Phys. Lett. **272**, 412 (1997).

[22] C. D. Ball and F. C. De Lucia, Direct Measurement of Rotationally Inelastic Cross Sections at Astrophysical and Quantum Collisional Temperatures, Phys. Rev. Lett. **81**, 305 (1998).

[23] C. D. Ball and F. C. De Lucia, Direct observation of Λ-doublet and hyperfine branching ratios for rotationally inelastic collisions of NO-He at 4.2 K, Chem. Phys. Lett. **300**, 227 (1999).

[24] I. Kozyryev, L. Baum, K. Matsuda, P. Olson, B. Hemmerling, and J. M. Doyle, Collisional relaxation of vibrational states of SrOH with He at 2 K, New J. Phys. **17**, 045003 (2015).

[25] C. I. Hancox, S. C. Doret, M. T. Hummon, R. V. Krems, and J. M. Doyle, Suppression of Angular Momentum Transfer in Cold Collisions of Transition Metal Atoms in Ground States with Nonzero Orbital Angular Momentum, Phys. Rev. Lett. **94**, 013201 (2005).

[26] C. I. Hancox, S. C. Doret, M. T. Hummon, L. Luo, and J. M. Doyle, Magnetic trapping of rare-earth atoms at millikelvin temperatures, Nature (London) **431**, 281 (2004).

[27] W. Campbell and J. Doyle, *Cooling, Trap Loading, and Beam Production Using a Cryogenic Helium Buffer Gas*, Cold Molecules: Theory, Experiment, Applications (CRC Press, Boca Raton, FL, 2009).

[28] R. C. Forrey, V. Kharchenko, N. Balakrishnan, and A. Dalgarno, Vibrational relaxation of trapped molecules, Phys. Rev. A **59**, 2146 (1999).

[29] C. Sommer, L. D. van Buuren, M. Motsch, S. Pohle, J. Bayerl, P. W. H. Pinkse, and G. Rempe, Continuous guided beams of slow and internally cold polar molecules, Faraday Discuss. **142**, 203 (2009).

[30] M. Zeppenfeld, B. G. U. Englert, R. Glöckner, A. Prehn, M. Mielenz, C. Sommer, L. D. van Buuren, M. Motsch, and G. Rempe, Sisyphus cooling of electrically trapped polyatomic molecules, Nature (London) **491**, 570 (2012).

[31] J. H. Brown and A. Carrington, *Rotational Spectroscopy of Diatomic Molecules* (Cambridge University Press, Cambridge, UK, 2003).

[32] R. N. Zare, *Angular Momentum: Understanding Spatial Aspects in Chemistry and Physics* (Wiley, New York, 1988).

[33] H. Pauly, *Atom, Molecule, and Cluster Beams I: Basic Theory, Production and Detection of Thermal Energy Beams* (Springer, New York, 2000).

[34] M. Yun, Y. Liu, L. Z. Deng, Q. Zhou, and J. P. Yin, Generation of CW cold CH_3CN molecular beam by a bent electrostatic quadrupole guiding: Monte-Carlo study, Front. Phys. China **3**, 19 (2008).

[35] W. C. Campbell, E. Tsikata, Hsin-I Lu, L. D. van Buuren, and J. M. Doyle, Magnetic Trapping and Zeeman Relaxation of NH ($X^3\Sigma^-$), Phys. Rev. Lett. **98**, 213001 (2007).

[36] M. J. Lu and J. D. Weinstein, Cold TiO ($X^3\Delta$)-He collisions, New J. Phys. **11**, 055015 (2009).